

# $^{13}\text{C}$ NMR Chemical Shift Prediction of the $\text{sp}^3$ Carbon Atoms in the $\alpha$ Position Relative to the Double Bond in Acyclic Alkenes

O. Ivanciuc,<sup>§</sup> J.-P. Rabine,<sup>†</sup> D. Cabrol-Bass,<sup>\*,†</sup> A. Panaye,<sup>‡</sup> and J. P. Doucet<sup>‡</sup>

Department of Organic Chemistry, Faculty of Chemical Technology, University "Politehnica" of Bucharest, Splaiul Independentei 313, 77206 Bucharest, Romania, LARTIC University of Nice-Sophia Antipolis, Parc Valrose 06108 Nice Cedex, France, and ITODYS, University of Paris 7 - Denis Diderot, 1 Rue Guy de la Brosse, 75005 Paris, France

Received November 13, 1996<sup>⊗</sup>

The  $^{13}\text{C}$  NMR chemical shift of  $\text{sp}^3$  carbon atoms situated in the  $\alpha$  position relative to the double bond in acyclic alkenes was estimated with multilayer feedforward artificial neural networks (ANNs) and multilinear regression (MLR), using as structural descriptors a topo-stereochemical code which characterizes the environment of the resonating carbon atom. The predictive ability of the two models was tested by the leave-20%-out cross-validation method. The neural model provides better results than the MLR model both in calibration and in cross-validation, demonstrating that there exists a nonlinear relationship between the structural descriptors and the investigated  $^{13}\text{C}$  NMR chemical shift and that the neural model is capable to capture such a relationship in a simple and effective way. A comparison between a general model for the estimation of the  $^{13}\text{C}$  NMR chemical shift and the ANN model indicates that general models are outperformed by more specific models, and in order to improve the predictions a possible way is to develop environment-specific models. The approach proposed in this paper can be used in automated spectra interpretation or computer-assisted structure elucidation to constrain the number of possible candidates generated from the experimental spectra.

## 1. INTRODUCTION

The growing interest in the application of Artificial Neural Networks (ANNs) in the field of computer-assisted spectral interpretation is a result of their demonstrated superiority over the traditional models.<sup>1</sup> The use of ANNs in spectra interpretation and structure elucidation is 2-fold, i.e., either for classification (recognition of structural characteristics from IR<sup>2–11</sup> or MS spectra,<sup>12–15</sup> joint IR- $^{13}\text{C}$ -NMR spectra<sup>1</sup> or IR-MS spectra<sup>16</sup>) or for a quantitative prediction of a certain atomic property (the chemical shift in  $^{13}\text{C}$  NMR spectra).<sup>17–28</sup>

In a previous paper<sup>28</sup> we have estimated the  $^{13}\text{C}$  NMR chemical shift of  $\text{sp}^2$  carbon atoms in acyclic alkenes with MultiLinear Regression (MLR) and MultiLayer Feedforward (MLF) ANN models, using as structural descriptor of the environment of the resonating carbon a Topo-Stereochemical Code (TSC) with 12 components allowing for a unique description of the topo-stereochemical location of the carbon atoms around the double bond. The study investigated the  $^{13}\text{C}$  NMR chemical shift of 130 acyclic alkenes with 244 structurally unique  $\text{sp}^2$  carbon atoms. The best calibration and Leave-20%-Out (L20%O) cross-validation results were obtained with networks provided with four hidden neurons. The standard deviation for calibration ranges between 0.59 and 0.63 ppm, while for the cross-validation it lies between 0.89 and 1.07 ppm, depending on the combination of hidden

and output activation functions used. Three types of activation functions were tested, namely the hyperbolic tangent ( $\tanh$ ) or a bell-shaped function ( $\text{Act}(z) = 1/(1+z^2)$ ) for the hidden layer and a linear or a  $\tanh$  function for the output layer. The best prediction results were provided by the networks with a  $\tanh$  hidden function and a linear output function, but from a statistical point of view it was not possible to choose a particular combination of activation functions against the others. The neural model which used the TSC description of the local structure of a  $\text{sp}^2$  carbon atom provided better predictions than the MLR model which used the same TSC structural descriptors, showing that there is a nonlinear dependence between the TSC descriptors and the chemical shift, and consequently the use of ANN is justified. It was found that the mean of the predictions of four networks with different pairs of activation functions exhibit a smaller number of outliers with lower residuals. Also, the ANN model was demonstrated to give better predictions than three general additive models for the calculation of the  $^{13}\text{C}$  NMR shift. This results indicate that in order to obtain better predictions for the  $^{13}\text{C}$  NMR chemical shift using simple models a promising option is to develop specific models for each type of chemical environment. The local environment description must take into account both the topological and stereochemical distribution of atoms in layers around the investigated atom.

In the present paper we extend the TSC description of the atomic environment in order to model the  $^{13}\text{C}$  NMR chemical shift for the  $\text{sp}^3$  carbon atoms situated in the  $\alpha$  position relative to a double bond in acyclic alkenes (denoted  $\alpha\text{-sp}^2$  carbon atoms). Their chemical shift (denoted by  $\alpha\text{-sp}^2\text{-CS}$ ) is estimated with neural networks provided with four types

\* Author to whom inquiries about the paper should be addressed.

† LARTIC University of Nice-Sophia Antipolis.

‡ University of Paris 7.

§ University "Politehnica" of Bucharest.

⊗ Abstract published in *Advance ACS Abstracts*, April 1, 1997.

of activation functions: the hyperbolic tangent or a bell-shaped function for the hidden layer, and the linear, the symmetric logarithmoid, or the hyperbolic tangent function for the output layer. The calibration and prediction performances of the neural model is compared with the results obtained with a MLR model, in order to be able to conclude on the existence of a nonlinear relationship between the structural descriptors and the chemical shift and on the opportunity of using neural networks for the  $^{13}\text{C}$  NMR chemical shift prediction. Also, the predictions of the neural model is compared with the estimations of a general additive model for the calculation of the  $^{13}\text{C}$  NMR chemical shift.

## 2. METHOD

**Data Set.** The studied population is formed by 136 alkenes that correspond to 243  $\alpha\text{-sp}^2$  carbon atoms with distinct environments. The structure and experimental  $^{13}\text{C}$  NMR chemical shift (in ppm) of the 243  $\alpha\text{-sp}^2$  carbon atoms used in the present investigation were taken from the literature and are reported in Table 1.

**Structural Coding.** A topological encoding of the atomic environment represents an efficient and simple description of the local (atomic) chemical structure in the case of highly flexible molecules. The geometry of acyclic molecules presents many local minima, making thus difficult to characterize in a simple way the local and global structure with geometric structural descriptors. Also, the identification of the ground state geometry is of little use in QSPR, because at the temperature where the physical properties are determined the molecules exist in many conformations, representing local energetic minima; their identification and description of the molecular population of each minima is computationally expensive, and for these reasons molecular dynamics computations are not routinely used in QSPR studies. We have to mention that a topological encoding of the atomic environment proved to be efficient both in MLR<sup>29</sup> and ANN<sup>19,20</sup> estimation of  $^{13}\text{C}$  NMR chemical shifts.

In the present study the topo-stereochemical description of the environment of the  $\alpha\text{-sp}^2$  resonating carbon atom considers all  $\text{sp}^3$ -hybridized carbon neighbors of type A, B, C, and D situated at 1, 2, 3, and 4 bonds away from the resonating atom. The four spheres of neighbors around a  $\alpha\text{-sp}^2$  resonating carbon (denoted  $\text{C}^*$ ) are depicted in Figure 1 according to their type resulting from the topo-stereochemical position relative to  $\text{C}^*$ . The use of an environment with a larger sphere of atoms does not add much information, because the influence on the chemical shift of the atoms situate at a distance greater than four bonds can be neglected.

In order to take into account the *Z*, *E* stereoisomerism around the double bond in the description of the environment of the resonating carbon, the sites within the sphere of four bonds around  $\text{C}^*$  are ordered into four classes: those directly linked to  $\text{C}^*$  and those linked through the gem, trans, and cis positions (see Figure 1). Within the first class the sites are further hierarchically ordered according to whether site A is occupied or not by a carbon atom, greater number of occupied B, and successively C and D locations. Once the environment is ordered, it is possible to construct a TSC vector which describes the topo-stereochemical environment. Each site is assigned a value equal to 1 if it is occupied by a carbon atom and a value equal to 0 otherwise. The TSC

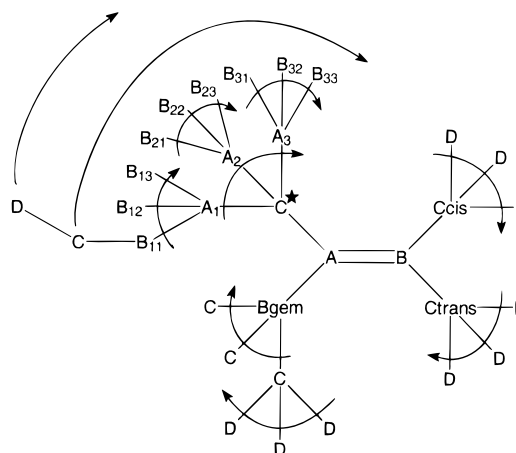


**Figure 1.** Description of sites in the topo-stereochemical code of the  $\alpha\text{-sp}^2$  carbon atoms. The resonating carbon atom is designated by  $\text{C}^*$ .

vector is made of 13 components, defined as follows:

$$\text{TSC}(1) = A_1 + A_2 + A_3$$

$$\text{TSC}(2) = B_{11} + B_{12} + B_{13}$$

$$\text{TSC}(3) = B_{21} + B_{22} + B_{23}$$

$$\text{TSC}(4) = B_{31} + B_{32} + B_{33}$$

$$\text{TSC}(5) = \sum C$$

$$\text{TSC}(6) = \sum D$$

$$\text{TSC}(7) = B_{\text{gem}}$$

$$\text{TSC}(8) = \sum C_{\text{gem}}$$

$$\text{TSC}(9) = \sum D_{\text{gem}}$$

$$\text{TSC}(10) = C_{\text{trans}}$$

$$\text{TSC}(11) = \sum D_{\text{trans}}$$

$$\text{TSC}(12) = C_{\text{cis}}$$

$$\text{TSC}(13) = \sum D_{\text{cis}}$$

The first class of sites is described by five parameters, while only two parameters are required to describe each of three other classes. As pointed out in our previous work, this encoding is not biunivocal but is justified by the limited interaction of C and D locations. Examples of the TSC vectors for some common substituents are presented in Table 2. The notation of the substituents is identical with the one used in Table 1.

**Network Architecture.** The present study used multilayer feedforward neural networks provided with a single hidden layer. The size of the input layer of the ANN is determined by the length of the code used to describe the environment of  $\alpha\text{-sp}^2$  carbon atom (i.e., 13 in the present study), and the number of neurons in the hidden layer was selected on the basis of systematic empirical trials in which ANNs with increasing number of hidden neurons were trained to predict the experimental  $^{13}\text{C}$  chemical shift values. Each network was provided with a bias neuron connected to all neurons in

the hidden and output layers, and one output neuron which provides the calculated value of the <sup>13</sup>C chemical shift.

**Activation Functions.** The most commonly used activation function in chemical applications of neural networks has a sigmoidal shape and takes values between 0 and 1. For large negative arguments its value is close to 0, and practice demonstrated that learning with the backpropagation algorithm is difficult in such conditions. To overcome this deficiency of the sigmoid function, the hyperbolic tangent (tanh) which takes values between -1 and 1 was used in the present study. For the hidden layer neurons a bell-shaped activation function, defined as  $\text{Act}(z) = 1/(1+z^2)$ , was investigated. The use of the bell activation function has a theoretical basis, because recently Kreinovich<sup>30</sup> demonstrated that an arbitrary nonlinear activation function in the hidden layer is sufficient to represent all functions by neural networks. This theorem opened the possibility to use new activation functions in the neural model. In a previous study<sup>28</sup> we have obtained good results with a bell-shaped hidden activation function; for the output layer the tanh and linear functions provided better results than the bell-shaped function.

Both the tanh and the sigmoid activation functions are very flat when the absolute value of the argument is greater than 10. Therefore, the derivative has an extremely small value, and this type of activation function has a poor sensitivity to large positive or negative arguments. This is an important cause of the very slow rates of convergence during the training of neural networks with algorithms that use the derivative of the activation function (e.g., the backpropagation algorithm). In such situations, a linear output function provides better quantitative estimations than a sigmoidal one; therefore, for the output layer it was investigated for both the linear and the tanh activation functions. A new type of activation function which overcomes the limitations of the sigmoid and tanh functions is the symmetric logarithmoid,<sup>31,32</sup> defined by the formula  $\text{Act}(z) = \text{sign}(z) \ln(1+|z|)$ . The symmetric logarithmoid (symlog) is a monotonically increasing function with the maximum sensitivity near zero and with a monotonically decreasing sensitivity away from zero, but because its output is not restricted to the range between -1 and 1 this function is not insensitive to large positive or negative arguments.

**Preprocessing of the Data.** Each component of the input (topo-stereochemical code) and output (chemical shift of the  $\alpha$ -sp<sup>2</sup> carbon) patterns was linearly scaled between -0.9 and 0.9. For the tanh output activation function the scaling is required by the range of values of the function, while for the unbounded functions (linear and symlog) the experience showed that a linear scaling improves the learning process.

**Learning Method.** The training of the ANNs was performed with the standard backpropagation method,<sup>33</sup> until the convergence was obtained, i.e., the correlation coefficient between experimental and calculated chemical shift values improved by less than 10<sup>-5</sup> in 100 epochs. One epoch corresponds to the presentation of one complete set of examples. The patterns were presented randomly to the network, and the weights were updated after the presentation of each pattern. Random values between -0.1 and 0.1 were used as initial weights. In order to evaluate the effect of the initial random weights ten different sets of random weights were generated for each network investigated. The momentum was set to 0.8 and the learning rate was set to

0.01 for all activation functions used, and it was maintained constant during the training phase. In all cases the networks converged in a few thousands epochs, and the final results were slightly influenced by the initial random set of weights.

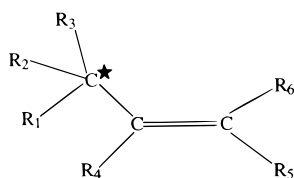
**Software Used.** The program which uses the standard backpropagation algorithm<sup>33</sup> was written in Borland C language and run on a PC486 DX2 at 66 MHz.

**Performance Indicators.** The performances of the neural networks were evaluated both for the model calibration and prediction. The quality of model calibration is estimated by comparing the calculated  $\alpha$ -sp<sup>2</sup> chemical shift during the training phase (CS<sub>calib</sub>) with the experimental target values (CS<sub>exp</sub>), while the predictive quality was estimated by a cross-validation method by comparing the predicted (CS<sub>pred</sub>) and experimental values. In order to compare the performance of the ANN models with the statistical results of the MLR equation, we have used the correlation coefficient  $r$  and the standard deviation  $s$  of the linear correlation between experimental and calibration or prediction chemical shifts, i.e.,  $\text{CS}_{\text{exp}} = a + b \times \text{CS}_{\text{calib/pred}}$ ,  $a$  and  $b$  being the linear regression coefficients.

**Cross-Validation.** In structure-property studies it is very important to take into consideration that feedforward neural networks are universal approximators: they are capable of arbitrarily accurate approximation to arbitrary mappings, when the network has a sufficiently large number of hidden units. Cybenko<sup>34</sup> and Funahashi<sup>35</sup> have shown that any continuous function can be approximated on a compact set with the uniform topology by a layered network with one hidden layer, while Hornik, Stinchcombe, and White<sup>36,37</sup> demonstrated that any measurable function can be approximated with a multilayer feedforward neural network.

The universal approximator feature of MLF ANN represents a property which must be considered with caution when using neural networks in developing structure-property models because a network with too many connections (adjustable parameters) can offer excellent calibration results for the patterns in the training set but will have poor performances for predicting the properties for new patterns, which were not present in the training set.

Because the scope of the present study is to develop a model that gives reliable predictions for new patterns that were not used in the calibration of the neural model, it is necessary to estimate the prediction capabilities of the ANNs with a cross-validation method and the leave-20%-out technique was used for this purpose. In the L20%O algorithm 20% of the patterns are selected at random from the complete data set and form the prediction set. In the following step the ANN model is calibrated with a learning set consisting of the remaining 80% of the data, and the neural model obtained in the calibration phase is used to predict the CS values for the patterns in the prediction set. This procedure is repeated five times, until all patterns are selected in a prediction set once and only once. A linear regression between experimental and predicted CS allows one to compare the prediction capabilities of different network architectures and sets of activation functions. The L20%O cross-validation procedure was repeated ten times with different sets of random initial weights for each size of the hidden layer and for each combination of hidden-output activation functions.

**Table 1.** Structure, Experimental  $^{13}\text{C}$  Chemical Shift, Calibration, and Prediction MLR and ANN Residuals for the Investigated  $\alpha\text{-sp}^2$  Carbon Atom, Denoted by C\* in the Figure

no.	R <sub>1</sub>	R <sub>2</sub>	R <sub>3</sub>	R <sub>4</sub>	R <sub>5</sub>	R <sub>6</sub>	exp (ppm)	ref <sup>a</sup>	MLR residuals		ANN residuals	
									calib	pred	calib	pred
1	H	H	H	H	H	H	19.4	K	-0.5	-1.4	-0.1	0.1
2	H	H	H	Me	H	H	24.2	K	-0.1	-0.4	0.9	1.4
3	H	H	H	H	Me	H	16.8	K	-3.8	-4.4	-1.4	-0.8
4	H	H	H	H	H	Me	11.4	K	-3.3	-4.0	-1.0	-1.1
5	H	H	H	Me	H	Me	17.1	K	-2.0	-1.9	0.3	-1.0
6	H	H	H	Me	Me	H	25.5	K	0.5	0.3	0.1	0.1
7	H	H	H	H	Me	Me	13.3	K	-2.1	-2.0	0.0	0.0
8	H	H	H	Me	Me	Me	20.4	K	0.6	0.5	-0.2	-0.5
9	Me	H	H	H	H	H	27.4	K	2.2	2.7	0.5	1.4
10	Me	H	H	Me	H	H	31.1	K	1.5	1.7	0.4	-0.6
11	H	H	H	Et	H	H	22.5	K	0.0	0.3	1.0	1.1
12	Me	H	H	H	Me	H	25.8	K	-0.1	0.1	-0.3	0.4
13	H	H	H	H	Et	H	17.3	K	-3.1	-3.3	-1.0	-1.3
14	Me	H	H	H	H	Me	20.3	K	0.3	0.7	-0.5	0.3
15	H	H	H	H	H	Et	12.0	K	-2.6	-2.6	-0.8	-0.8
16	Me	H	H	Me	Me	H	32.6	C	2.3	2.2	-0.2	-0.5
17	H	H	H	Et	H	Me	15.5	C	-1.7	-1.7	0.6	0.6
18	H	H	H	H	Et	Me	13.3	C	-1.9	-2.1	0.1	-0.4
19	Me	H	H	Me	H	Me	24.7	C	0.2	0.1	0.1	-0.5
20	H	H	H	Et	Me	H	22.9	C	-0.3	-0.3	0.9	0.3
21	H	H	H	H	Me	Et	13.0	C	-2.4	-1.9	-0.3	0.4
22	Me	H	H	H	Me	Me	21.5	C	0.8	0.6	0.1	-0.1
23	H	H	H	Me	H	Et	17.5	C	-1.7	-1.6	-0.1	-0.2
24	H	H	H	Me	Et	H	25.7	C	0.8	1.2	-0.3	-0.2
25	Me	H	H	Me	Me	Me	27.7	C	2.5	2.8	-1.1	0.9
26	H	H	H	Et	Me	Me	17.9	C	-0.1	0.0	0.2	-0.2
27	H	H	H	Me	Me	Et	20.6	C	0.8	0.6	-0.1	0.2
28	H	H	H	Me	Et	Me	19.9	C	0.2	0.0	-0.9	-1.2
29	Me	Me	H	H	H	H	32.7	K	2.2	2.4	0.1	0.0
30	Me	Me	H	Me	H	H	35.5	C	0.5	0.4	-0.3	-1.3
31	H	H	H	iPr	H	H	20.1	C	-0.5	-0.3	0.0	-0.2
32	Me	H	H	Et	H	H	28.1	K	0.3	0.4	-0.5	-0.4
33	Me	Me	H	H	H	Me	26.4	H	1.0	1.2	-1.5	-2.8
34	H	H	H	H	H	iPr	12.3	H	-2.3	-2.3	-1.2	-0.4
35	Me	H	H	H	Et	H	25.9	K	0.2	0.4	0.0	0.4
36	Me	H	H	H	H	Et	20.7	K	0.8	0.8	0.0	0.2
37	Me	Me	H	Me	Me	H	37.3	K	1.7	1.9	-0.4	-0.1
38	H	H	H	iPr	H	Me	13.1	H	-2.2	-2.3	-0.7	-1.2
39	H	H	H	H	iPr	Me	13.0	H	-2.1	-1.4	-0.2	-0.3
40	Me	Me	H	Me	H	Me	28.5	H	-1.2	-1.1	-1.9	-2.7
41	H	H	H	iPr	Me	H	17.8	H	-3.4	-3.3	-1.2	-2.3
42	H	H	H	H	Me	iPr	12.4	H	-2.8	-2.6	-1.0	-0.8
43	Me	H	H	Me	Et	H	32.5	C	2.4	2.6	-0.4	-0.5
44	H	H	H	Et	H	Et	15.7	C	-1.5	-1.6	0.1	0.1
45	Me	H	H	H	Et	Me	21.3	C	0.7	0.7	-0.1	0.7
46	Me	H	H	Me	H	Et	24.9	C	0.5	0.8	-0.1	0.2
47	H	H	H	Et	Et	H	22.9	C	-0.1	-0.3	0.2	0.4
48	Me	H	H	H	Me	Et	21.2	C	0.5	0.7	0.2	0.6
49	Me	Me	H	H	Me	Me	27.5	C	1.4	1.7	-0.8	-1.6
50	H	H	H	Me	H	iPr	17.7	C	-1.4	-1.6	-0.6	-0.4
51	H	H	H	Me	iPr	H	25.7	C	1.1	1.5	-0.8	-0.7
52	Me	H	H	Et	Me	Me	25.2	C	1.9	2.2	0.5	0.6
53	H	H	H	Me	Et	Et	20.0	C	0.4	0.9	-0.9	-0.6
54	Me	Me	Me	H	H	H	33.8	K	-2.0	-1.9	0.2	-0.9
55	Me	Me	Me	Me	H	H	36.0	K	-4.3	-4.1	0.3	0.8
56	H	H	H	tBu	H	H	19.6	K	0.9	0.8	0.6	-0.3
57	Me	Me	H	Et	H	H	34.3	C	1.2	1.4	-1.1	0.2
58	Me	H	H	iPr	H	H	27.1	C	1.1	1.3	0.6	0.7
59	Me	Me	Me	H	Me	H	33.1	H	-3.4	-3.4	-0.4	0.0
60	H	H	H	H	tBu	H	18.0	H	-2.0	-1.9	-0.9	-1.2
61	Me	Me	Me	H	H	Me	33.4	H	2.8	2.7	2.0	3.3
62	H	H	H	H	H	tBu	14.3	H	-0.3	-0.3	0.0	0.2
63	Me	Me	H	H	Et	H	31.1	C	0.1	-0.1	-0.7	-0.1
64	Me	H	H	H	iPr	H	25.7	C	0.1	0.3	-0.2	0.0

**Table 1** (Continued)

no.	R <sub>1</sub>	R <sub>2</sub>	R <sub>3</sub>	R <sub>4</sub>	R <sub>5</sub>	R <sub>6</sub>	exp (ppm)	ref <sup>a</sup>	MLR residuals		ANN residuals	
									calib	pred	calib	pred
65	Me	Me	H	H	H	Et	26.6	C	1.4	1.0	-1.2	-1.9
66	Me	H	H	H	H	iPr	20.8	C	0.9	1.0	-0.1	0.4
67	Me	Me	H	Et	Me	H	35.2	H	1.5	1.9	0.2	-1.2
68	Me	H	H	iPr	H	Me	22.4	H	1.8	1.9	2.5	1.8
69	H	H	H	H	iPr	Et	13.8	H	-1.2	-1.2	0.4	1.3
70	Me	Me	H	Et	H	Me	29.2	H	1.3	1.4	-0.1	-0.4
71	Me	H	H	iPr	Me	H	24.2	H	-2.4	-3.2	-0.3	-1.1
72	H	H	H	H	Et	iPr	12.7	H	-2.4	-2.8	-0.9	-0.9
73	Me	Me	Me	H	Me	Me	32.2	C	0.8	1.2	0.5	0.0
74	H	H	H	Me	H	tBu	18.8	C	-0.3	-0.2	0.1	-1.1
75	H	H	H	Me	tBu	H	28.0	C	3.5	4.0	0.5	2.4
76	Me	Me	Me	Me	Me	H	36.1	C	-4.8	-4.9	-1.2	-3.1
77	H	H	H	tBu	H	Me	13.6	C	0.1	0.5	0.0	2.5
78	H	H	H	H	tBu	Me	12.4	C	-2.4	-1.8	-0.9	-1.1
79	Me	Me	H	iPr	H	H	34.2	D	3.0	3.2	0.0	0.8
80	Me	Me	H	H	iPr	H	31.6	K	0.8	1.1	0.3	0.5
81	Me	Me	H	H	H	iPr	27.9	K	2.7	2.1	-0.2	-1.6
82	Me	Me	Me	H	Et	H	32.6	C	-3.7	-3.9	-0.4	-1.1
83	Me	H	H	H	tBu	H	25.8	C	0.4	0.3	-0.1	0.5
84	Me	Me	Me	H	H	Et	33.2	C	2.7	2.9	1.7	3.0
85	Me	H	H	H	H	tBu	21.7	C	1.9	2.0	0.5	1.4
86	Me	Me	Me	iPr	H	H	38.3	D	1.8	2.4	0.4	0.3
87	Me	Me	H	tBu	H	H	30.2	D	0.9	1.3	-2.0	-3.1
88	Me	Me	Me	tBu	H	H	39.2	D	4.6	5.1	1.1	0.8
89	Me	Me	Me	Me	tBu	Me	36.8	K	1.7	2.4	-0.6	4.0
90	H	H	H	tBu	Me	tBu	19.5	K	5.6	7.2	0.4	5.2
91	Et	H	H	H	H	H	36.2	C	3.9	4.0	-0.6	0.4
92	Et	H	H	Me	H	H	40.3	C	3.5	3.4	-0.4	-0.7
93	H	H	H	nPr	H	H	22.4	C	-1.0	-1.4	-0.1	-0.1
94	Et	H	H	H	Me	H	35.0	C	2.1	2.4	-0.2	-0.4
95	H	H	H	H	nPr	H	17.9	C	-2.6	-2.7	-0.5	-0.4
96	Et	H	H	H	H	Me	29.2	C	2.2	2.3	-0.1	-0.7
97	H	H	H	H	H	nPr	12.8	C	-1.9	-1.9	-0.1	0.6
98	Et	H	H	Me	Me	H	42.2	C	4.8	4.9	-1.0	-0.6
99	H	H	H	nPr	H	Me	15.5	C	-2.6	-2.8	-0.3	-0.3
100	H	H	H	H	nPr	Me	13.3	C	-1.9	-1.8	0.1	0.3
101	Et	H	H	Me	H	Me	33.7	C	2.1	1.7	-0.3	0.4
102	H	H	H	nPr	Me	H	23.4	C	-0.6	-0.8	0.2	0.4
103	H	H	H	H	Me	nPr	13.3	C	-2.1	-1.6	0.0	0.7
104	Et	H	H	H	Me	Me	30.4	C	2.7	3.0	0.4	-0.4
105	H	H	H	Me	H	nPr	17.7	C	-1.5	-1.7	0.1	0.1
106	H	H	H	Me	nPr	H	25.7	C	0.9	0.9	-0.2	-0.5
107	Et	H	H	Me	Me	Me	36.8	C	4.7	4.8	0.3	-1.0
108	H	H	H	nPr	Me	Me	18.4	C	-0.5	0.0	-0.6	0.8
109	H	H	H	Me	Me	nPr	20.6	C	0.8	0.9	-0.1	0.0
110	H	H	H	Me	nPr	Me	20.2	C	0.5	0.9	-0.6	-0.8
111	Et	Me	H	H	H	H	39.7	C	2.1	1.9	0.5	0.2
112	Et	Me	H	Me	H	H	44.3	D	2.3	2.8	1.9	3.1
113	H	H	H	sBu	H	H	20.5	D	-0.9	-1.1	-0.3	-0.8
114	Et	H	H	Et	H	H	38.7	C	3.9	3.2	0.2	-0.1
115	Me	H	H	nPr	H	H	29.0	C	0.3	0.1	-0.9	0.1
116	Et	Me	H	H	Me	H	38.7	C	0.5	-0.1	0.8	1.6
117	H	H	H	H	sBu	H	17.9	C	-2.3	-2.5	-0.6	-0.3
118	Et	Me	H	H	H	Me	33.2	C	0.9	0.8	0.5	1.5
119	H	H	H	H	H	sBu	13.0	C	-1.7	-1.3	-0.6	-0.2
120	Et	H	H	H	Et	H	35.1	H	2.4	2.7	-0.2	-0.5
121	Me	H	H	H	nPr	H	25.9	H	0.2	0.0	0.0	0.7
122	Et	H	H	H	H	Et	29.6	H	2.6	2.4	-0.3	-0.3
123	Me	H	H	H	H	nPr	20.9	H	0.9	1.0	0.1	0.5
124	Et	Me	H	Me	Me	H	45.4	H	2.8	1.8	0.6	2.7
125	H	H	H	sBu	H	Me	12.1	H	-4.1	-4.2	-2.3	-3.7
126	H	H	H	H	sBu	Me	13.2	H	-1.9	-1.9	0.0	-0.1
127	Et	Me	H	Me	H	Me	35.9	H	-1.0	-0.7	-0.4	1.7
128	H	H	H	sBu	Me	H	17.9	H	-4.3	-4.3	-2.1	-2.1
129	H	H	H	H	Me	sBu	12.8	H	-2.5	-2.3	-0.7	-0.5
130	Et	Me	Me	H	H	H	36.7	C	-6.2	-7.1	-0.4	-1.4
131	Et	Me	Me	Me	H	H	39.2	C	-8.2	-9.5	-0.7	-1.2
132	H	H	H	tPent	H	H	19.4	C	-0.2	-0.4	-0.3	-1.4
133	Et	Me	H	Et	H	H	43.3	D	3.2	3.7	0.4	2.8
134	Me	H	H	sBu	H	H	27.5	D	0.8	0.8	-0.1	0.5
135	Et	Me	Me	tBu	H	H	42.8	D	1.2	1.4	-1.1	-0.3
136	Me	Me	Me	tPent	H	H	39.1	D	3.6	4.2	0.6	0.9
137	iPr	H	H	H	H	H	43.6	C	4.2	5.0	-0.6	-0.2

Table 1 (Continued)

no.	R <sub>1</sub>	R <sub>2</sub>	R <sub>3</sub>	R <sub>4</sub>	R <sub>5</sub>	R <sub>6</sub>	exp (ppm)	ref <sup>a</sup>	MLR residuals		ANN residuals	
									calib	pred	calib	pred
138	iPr	H	H	Me	H	H	48.0	C	4.2	3.4	0.6	1.2
139	H	H	H	iBu	H	H	22.2	C	-2.0	-2.0	-1.1	0.9
140	iPr	H	H	H	Me	H	42.3	C	2.3	1.7	-0.9	-1.1
141	H	H	H	H	iBu	H	17.9	C	-2.5	-2.6	-0.4	-0.3
142	iPr	H	H	H	H	Me	36.3	C	2.1	2.8	0.7	0.8
143	H	H	H	H	H	iBu	12.8	C	-1.8	-2.0	0.0	0.4
144	iPr	H	H	H	Me	Me	37.5	C	2.8	3.2	0.8	-0.4
145	H	H	H	Me	iBu	H	25.8	C	1.0	0.7	-0.1	0.1
146	H	H	H	Me	H	iBu	17.8	C	-1.4	-1.6	0.2	0.2
147	iPr	Me	H	H	H	H	44.4	C	-0.3	-0.4	0.5	1.3
148	Et	Et	H	H	H	H	47.9	C	7.2	7.9	0.5	2.6
149	Et	Et	H	Me	H	H	51.4	C	6.2	7.8	-0.2	-2.6
150	H	H	H	CH(Et) <sub>2</sub>	H	H	18.1	C	-4.2	-4.5	-3.5	-4.0
151	Et	H	H	H	nPr	H	35.3	H	2.5	2.3	-0.1	-0.2
152	Et	H	H	H	H	nPr	29.8	H	2.7	2.7	-0.2	0.2
153	iPr	Me	Me	Me	H	H	42.8	D	-11.5	-13.4	0.1	-0.8
154	H	H	H	C(Me) <sub>2</sub> iPr	H	H	20.8	D	0.4	0.7	0.6	-0.4
155	tBu	H	H	H	H	H	48.9	K	2.6	1.6	0.9	1.2
156	tBu	H	H	Me	H	H	51.9	C	1.0	0.0	-0.1	0.2
157	H	H	H	neoPent	H	H	25.2	C	0.1	0.1	0.9	3.3
158	tBu	Me	Me	Me	H	H	44.7	D	-16.7	-17.6	-0.1	-0.8
159	H	H	H	C(Me) <sub>2</sub> tBu	H	H	25.2	D	3.9	4.8	4.3	6.7
160	tBu	H	H	Me	tBu	H	55.7	C	4.8	3.1	-0.5	-0.6
161	Me	Me	Me	H	neoPent	Me	31.7	C	0.6	1.0	0.1	1.3
162	H	H	H	neoPent	H	tBu	20.0	C	0.3	0.4	0.4	2.3
163	tBu	Me	Me	iPr	H	H	46.1	D	-11.5	-14.6	-0.7	-3.2
164	Me	Me	H	C(Me) <sub>2</sub> tBu	H	H	34.3	D	2.4	2.5	-1.2	-1.3
165	tBu	Me	Me	tBu	H	H	48.2	D	-7.5	-11.1	0.3	-1.7
166	Me	Me	Me	C(Me) <sub>2</sub> tBu	H	H	38.8	D	1.6	2.0	0.2	-1.3
167	tBu	H	H	neoPent	H	H	51.4	C	-0.2	0.0	-0.2	-3.8
168	tBu	H	H	neoPent	neoPent	neoPent	47.4	K	0.7	1.9	0.2	-1.9
169	nPr	H	H	H	H	H	33.8	K	1.6	1.6	-0.2	-0.5
170	nPr	H	H	H	Me	H	32.6	C	-0.3	-0.3	-0.4	0.0
171	H	H	H	H	nBu	H	17.9	C	-2.5	-2.7	-0.4	-0.7
172	nPr	H	H	H	H	Me	26.8	C	-0.2	-0.2	-0.2	-0.8
173	H	H	H	H	H	nBu	12.7	C	-1.9	-1.3	-0.1	0.4
174	nPr	H	H	Me	H	H	37.8	C	1.2	1.4	-0.3	-0.7
175	H	H	H	nBu	H	H	22.4	C	-0.9	-0.2	0.0	0.5
176	nPr	H	H	H	Et	H	32.8	H	0.1	-0.3	-0.2	-0.2
177	Me	H	H	H	nBu	H	26.1	H	0.3	0.6	0.1	0.4
178	nPr	H	H	H	H	Et	27.3	H	0.4	0.3	-0.1	-0.2
179	Me	H	H	H	H	nBu	21.0	H	1.0	1.0	0.2	-0.1
180	nPr	H	H	H	Me	Me	28.0	C	0.4	0.6	-0.2	0.0
181	H	H	H	Me	H	nBu	17.6	C	-1.5	-1.4	0.1	0.0
182	H	H	H	Me	nBu	H	25.7	C	0.9	1.3	-0.2	-0.1
183	nPr	Me	H	Me	H	H	41.1	C	-0.8	-1.7	0.2	0.2
184	H	H	H	sPent	H	H	18.9	C	-2.5	-2.7	-1.9	-2.4
185	nPr	H	H	Et	H	H	36.0	S	1.3	0.4	0.2	0.0
186	Me	H	H	nBu	H	H	30.0	S	1.4	1.4	0.2	1.3
187	nPr	Me	H	H	H	H	37.8	C	0.2	0.6	0.1	0.2
188	sBu	H	H	H	H	H	41.3	C	2.1	2.1	-1.0	-0.5
189	nPr	H	H	H	nPr	H	32.9	H	0.2	0.6	-0.1	-0.1
190	Et	H	H	H	nBu	H	35.3	H	2.6	2.9	0.0	-0.3
191	nPr	H	H	H	H	nPr	27.5	H	0.5	0.8	0.0	0.3
192	Et	H	H	H	H	nBu	29.9	H	2.9	3.3	0.0	-0.2
193	tPent	H	H	H	H	H	46.3	C	0.0	0.6	-1.0	-1.0
194	iBu	H	H	H	H	H	31.9	C	-0.3	-0.6	0.8	0.0
195	nPr	H	H	H	nBu	H	32.5	C	-0.2	-0.6	-0.5	-0.5
196	nPr	H	H	H	H	nBu	27.5	H	0.6	0.9	0.1	0.4
197	nBu	H	H	H	H	H	34.0	C	1.6	1.6	0.0	-0.1
198	nBu	H	H	H	Me	H	33.2	H	0.1	-0.2	-0.3	0.2
199	H	H	H	H	nPent	H	17.8	H	-2.6	-2.8	-0.5	-0.8
200	nBu	H	H	H	H	Me	27.4	H	0.1	0.0	0.0	0.0
201	H	H	H	H	H	nPent	12.6	H	-2.0	-2.0	-0.2	0.5
202	nBu	H	H	H	Et	H	32.8	C	-0.2	0.1	-0.4	-0.3
203	Me	H	H	H	nPent	H	25.8	C	0.0	-0.2	-0.2	0.5
204	nBu	H	H	H	H	Et	27.7	H	0.5	0.8	0.1	0.4
205	Me	H	H	H	H	nPent	21.0	H	1.0	0.8	0.2	0.2
206	nBu	H	H	H	nPr	H	32.8	C	-0.1	0.2	-0.3	-0.2
207	Et	H	H	H	nPent	H	35.0	C	2.2	2.3	-0.4	-0.7
208	nBu	H	H	H	H	nPr	27.8	H	0.7	0.8	0.3	0.4
209	Et	H	H	H	H	nPent	29.9	H	2.9	3.3	0.0	-0.2
210	2-MeBu	H	H	H	Me	Me	25.9	C	-1.9	-2.5	-0.4	-0.6

**Table 1** (Continued)

no.	R <sub>1</sub>	R <sub>2</sub>	R <sub>3</sub>	R <sub>4</sub>	R <sub>5</sub>	R <sub>6</sub>	exp (ppm)	ref <sup>a</sup>	MLR residuals		ANN residuals	
									calib	pred	calib	pred
211	H	H	H	Me	H	3-MePent	17.6	C	-1.5	-1.4	0.1	-0.6
212	H	H	H	Me	3-MePent	H	25.7	C	0.9	0.9	-0.2	-0.5
213	nPent	H	H	Me	H	H	38.1	C	1.3	1.6	0.6	0.3
214	H	H	H	nHex	H	H	22.4	C	-0.9	-1.2	0.0	-0.2
215	nPent	H	H	H	Me	H	33.2	H	0.1	0.1	-0.3	0.4
216	H	H	H	H	nHex	H	17.8	H	-2.6	-1.8	-0.5	0.0
217	nPent	H	H	H	H	Me	27.4	H	0.2	0.5	0.1	-0.5
218	H	H	H	H	H	nHex	12.7	H	-2.0	-2.4	-0.2	0.0
219	nPent	H	H	H	Et	H	33.2	H	0.3	0.6	0.1	0.2
220	Me	H	H	H	nHex	H	26.2	H	0.4	0.6	0.2	0.6
221	nPent	H	H	H	H	Et	27.8	H	0.6	0.7	0.2	0.3
222	Me	H	H	H	H	nHex	21.1	H	1.1	1.1	0.3	0.2
223	nHex	H	H	H	Me	H	32.8	C	-0.2	-0.2	-0.6	-0.4
224	H	H	H	H	nHept	H	17.9	C	-2.5	-2.9	-0.4	-0.1
225	nHex	H	H	H	H	Me	27.5	H	0.2	0.2	0.1	0.2
226	H	H	H	H	H	nHept	12.8	H	-1.9	-1.9	-0.1	0.6
227	nHex	H	H	Me	H	H	38.1	C	1.2	1.0	0.5	-1.0
228	H	H	H	nHept	H	H	22.4	C	-1.0	-1.1	-0.1	1.4
229	nPent	H	H	H	H	H	34.0	C	1.6	1.4	0.0	-0.1
230	nHept	H	H	H	H	H	34.0	S	1.6	1.6	0.0	0.4
231	nOct	H	H	Me	H	H	38.0	S	1.2	1.0	0.5	-1.0
232	H	H	H	nNon	H	H	22.0	S	-1.3	-1.4	-0.4	1.1
233	nDec	H	H	H	H	H	34.0	C	1.6	1.6	0.0	-0.1
234	nUndec	H	H	H	H	H	34.0	S	1.6	1.6	0.0	-0.1
235	nTridec	H	H	H	H	H	34.0	S	1.6	1.9	0.0	0.1
236	nPentadec	H	H	H	H	H	34.0	S	1.6	1.9	0.0	0.1
237	nBu	Et	Me	H	H	H	39.5	Sc	-6.8	-9.1	-0.5	-0.6
238	nBu	Et	Et	H	H	H	42.1	Sc	0.7	1.1	-0.2	-0.6
239	nBu	nPr	Me	H	H	H	39.5	Sc	-6.7	-6.7	0.0	0.3
240	nBu	nPr	Et	H	H	H	42.0	Sc	0.7	0.8	0.1	-0.2
241	nBu	nBu	Me	H	H	H	39.3	Sc	-2.3	-3.2	-1.3	-2.0
242	nBu	nPr	nPr	H	H	H	41.9	Sc	0.7	1.1	0.3	1.7
243	nBu	nBu	Et	H	H	H	41.9	Sc	0.3	0.7	1.3	2.0

<sup>a</sup> C: Couperus, P. A.; Clague, A. D. H.; van Dongen, J. P. C. M. <sup>13</sup>C Chemical Shifts of some Model Olefins. *Org. Magn. Reson.* **1976**, 8, 246–431. D: Dubois, J.-E.; Carabedian, M. Modelling of the Alkyl Environment Effects on <sup>13</sup>C Chemical Shifts. *Org. Magn. Reson.* **1980**, 5, 264–271. F: Friedel, R. A.; Retcofsky, H. L. Carbon-13 Nuclear Magnetic Resonance Spectra of Olefins and Other Hydrocarbons, *J. Am. Chem. Soc.* **1963**, 85, 1300–1306. H: de Haan, J. W.; van de Ven, L. J. M. Configurations and Conformations in Acyclic, Unsaturated Hydrocarbons. A <sup>13</sup>C NMR Study. *Org. Magn. Reson.* **1973**, 5, 147–153. K: Kalinowski, H.-O.; Berger, S.; Braun, S. *Carbon-13 NMR Spectroscopy*; John Wiley & Sons: Chichester, 1988; pp 132–134. S: <sup>13</sup>C NMR Database from Bio-Rad Laboratories, Inc. Sadtler Division, Philadelphia PA 19104. Sc: Schwartz, R. M.; Rabjohn, N. <sup>13</sup>C NMR Chemical Shifts of Some highly-branched Acyclic Compounds. *Org. Magn. Reson.* **1980**, 13, 9–13.

**Table 2.** Selected Examples of Topo-Stereochemical Codes for the α-sp<sup>2</sup> Carbon Atoms<sup>a</sup>

no.	R <sub>1</sub>	R <sub>2</sub>	R <sub>3</sub>	R <sub>4</sub>	R <sub>5</sub>	R <sub>6</sub>	TSC												
							1	2	3	4	5	6	7	8	9	10	11	12	13
67	Me	Me	H	Et	Me	H	2	0	0	0	0	0	1	1	0	1	0	0	0
68	Me	H	H	iPr	H	Me	1	0	0	0	0	0	1	2	0	0	0	1	0
87	Me	Me	H	tBu	H	H	2	0	0	0	0	0	1	3	0	0	0	0	0
136	Me	Me	Me	tPent	H	H	3	0	0	0	0	0	1	3	1	0	0	0	0
154	H	H	H	C(Me) <sub>2</sub> iPr	H	H	0	0	0	0	0	0	1	3	2	0	0	0	0
167	tBu	H	H	neoPent	H	H	1	3	0	0	0	0	1	1	3	0	0	0	0
198	nBu	H	H	H	Me	H	1	1	0	0	1	1	0	0	0	1	0	0	0
219	nPent	H	H	H	Et	H	1	1	0	0	1	1	0	0	0	1	1	0	0
221	nPent	H	H	H	H	Et	1	1	0	0	1	1	0	0	0	0	1	1	1
222	Me	H	H	H	H	nHex	1	0	0	0	0	0	0	0	0	0	1	1	1
225	nHex	H	H	H	H	Me	1	1	0	0	1	1	0	0	0	0	1	0	0
227	nHex	H	H	Me	H	H	1	1	0	0	1	1	1	0	0	0	0	0	0
237	nBu	Et	Me	H	H	H	3	1	1	0	1	1	0	0	0	0	0	0	0
239	nBu	nPr	Me	H	H	H	3	1	1	0	2	1	0	0	0	0	0	0	0
240	nBu	nPr	Et	H	H	H	3	1	1	1	2	1	0	0	0	0	0	0	0
242	nBu	nPr	nPr	H	H	H	3	1	1	1	3	1	0	0	0	0	0	0	0
243	nBu	nBu	Et	H	H	H	3	1	1	1	2	2	0	0	0	0	0	0	0

<sup>a</sup> The identification numbers from column 1 matches those from Table 1.

### 3. RESULTS AND DISCUSSION

**Neural Networks Architecture.** The MLF networks trained with the backpropagation algorithm have a number of factors that influence their performance: the number of

hidden neurons, the activation functions of the hidden and output layers, the initial set of weights, the learning rates, and the momentum factor. A number of experiments was designed in order to study the influence of all the above factors on the estimation of α-sp<sup>2</sup>-CS. The number of hidden

**Table 3.** Calibration Results for the Estimation of the  $\alpha$ -sp<sup>2</sup>-CS with Neural Networks<sup>a</sup>

network specifications	<i>H</i>	<i>r</i> <sub>min</sub>	<i>r</i> <sub>max</sub>	<i>r</i> <sub>mean</sub>	<i>s</i> <sub>min</sub>	<i>s</i> <sub>max</sub>	<i>s</i> <sub>mean</sub>	<i>t</i> <sub>mean</sub> (s)
Act(Hidden)=tanh	1	0.9824	0.9824	0.9824	1.852	1.852	1.852	11
Act(Out)=linear	2	0.9930	0.9931	0.9930	1.166	1.170	1.168	91
	3	0.9938	0.9963	0.9957	0.855	1.101	0.921	415
	4	0.9964	0.9973	0.9970	0.725	0.841	0.769	822
	5	0.9972	0.9982	0.9977	0.602	0.748	0.664	984
	6	0.9979	0.9986	0.9981	0.527	0.644	0.603	1427
Act(Hidden)=tanh	1	0.9802	0.9802	0.9802	1.962	1.962	1.962	59
Act(Out)=symlog	2	0.9921	0.9921	0.9921	1.243	1.244	1.243	194
	3	0.9942	0.9950	0.9949	0.989	1.065	0.999	390
	4	0.9960	0.9965	0.9962	0.828	0.888	0.865	707
	5	0.9968	0.9974	0.9971	0.708	0.791	0.751	1346
	6	0.9968	0.9983	0.9976	0.575	0.797	0.685	1587
Act(Hidden)=tanh	1	0.9805	0.9805	0.9805	1.949	1.949	1.949	30
Act(Out)=tanh	2	0.9915	0.9915	0.9915	1.292	1.293	1.292	164
	3	0.9934	0.9944	0.9942	1.046	1.137	1.068	351
	4	0.9948	0.9963	0.9960	0.855	1.012	0.887	647
	5	0.9950	0.9974	0.9966	0.712	0.992	0.815	980
	6	0.9954	0.9984	0.9973	0.567	0.945	0.721	1737
Act(Hidden)=bell	1	0.9824	0.9824	0.9824	1.854	1.854	1.854	24
Act(Out)=linear	2	0.9919	0.9928	0.9923	1.183	1.256	1.227	123
	3	0.9937	0.9959	0.9950	0.892	1.107	0.984	364
	4	0.9959	0.9975	0.9967	0.707	0.896	0.807	436
	5	0.9950	0.9984	0.9976	0.557	0.990	0.679	672
	6	0.9978	0.9987	0.9983	0.515	0.653	0.574	1025
Act(Hidden)=bell	1	0.9634	0.9817	0.9799	1.889	2.655	1.965	99
Act(Out)=symlog	2	0.9912	0.9959	0.9922	1.180	1.315	1.234	199
	3	0.9934	0.9953	0.9948	0.962	1.138	1.006	334
	4	0.9959	0.9968	0.9964	0.791	0.893	0.842	741
	5	0.9966	0.9983	0.9972	0.573	0.812	0.740	875
	6	0.9972	0.9985	0.9981	0.536	0.744	0.616	1625
Act(Hidden)=bell	1	0.9641	0.9820	0.9784	1.872	2.634	2.024	120
Act(Out)=tanh	2	0.9907	0.9924	0.9919	1.218	1.346	1.257	307
	3	0.9941	0.9948	0.9945	1.014	1.071	1.039	531
	4	0.9942	0.9963	0.9955	0.848	1.070	0.937	656
	5	0.9960	0.9978	0.9970	0.653	0.880	0.761	641
	6	0.9961	0.9987	0.9977	0.509	0.876	0.665	1192

<sup>a</sup> The table reports the network specifications, number of hidden neurons (*H*), minimum, maximum, and mean correlation coefficient (*r*), and standard deviation (*s*) of the linear regression between the experimental and computed values of  $\alpha$ -sp<sup>2</sup>-CS and the mean time of training (*t*<sub>mean</sub>). The mean of the correlation coefficient, standard deviation, and training time is computed for ten simulations with different random initial weights.

neurons was varied between 1 and 6, and the following combinations of hidden and output activation functions were used: (tanh, linear), (tanh, symlog), (tanh, tanh), (bell, linear), (bell, symlog), (bell, tanh). In order to investigate the effect of the initial set of weights, each type of network was trained 10 times with a different set of random initial weights each time.

The results obtained for the calibration of the ANNs are presented in Table 3. For each pair of activation functions and a number of hidden neurons Table 3 gives the minimum, maximum, and mean value of the correlation coefficient and standard deviation of the linear equation which correlates the experimental and calculated  $\alpha$ -sp<sup>2</sup>-CS; the last column reports the mean time of computation (in seconds) for the ten runs. There was not a single case of network that did not converge in a reasonable amount of time, and as is apparent from Table 3 the difference between *s*<sub>min</sub> and *s*<sub>max</sub> for ten simulations is small, showing that consistent results are obtained for each set of simulations. On the other hand, in many cases, *s*<sub>min</sub> for a network with *n* hidden neurons is smaller than *s*<sub>max</sub> for the network with *n*+1 neurons provided with the same pair of activation functions. Thus it seems important that in QSPR applications of ANNs one should not limit the investigation to a single simulation with one set of random initial weights, in order to identify the optimum set of weights for a given number of hidden neurons. For all the networks with a dimension of the hidden layer

between four and six neurons *r*<sub>max</sub> lies between 0.996 and 0.999 and *s*<sub>min</sub> takes values between 0.5 and 0.9. The calibration results improve as the number of hidden neurons increase, together with a substantial increase of the computational time.

In order to establish the optimal size of the hidden layer and to obtain information concerning the predictive power of the ANNs, the L20%O cross-validation technique was applied for each network. Selected results of the L20%O cross-validation experiments are presented in Table 4. The statistical indices of the correlation between experimental and predicted  $\alpha$ -sp<sup>2</sup>-CS improve with the increase of the number of hidden neurons, with a smaller improvement between four and six neurons. In some cases it can be observed as a small degradation of the prediction performances when the number of hidden neurons increases over four (tanh, linear) or five (tanh, symlog). In the cross-validation experiments for all the networks with a dimension of the hidden layer between four and six neurons *r*<sub>max</sub> takes values between 0.986 and 0.991, and *s*<sub>min</sub> lies between 1.6 and 1.3. The networks provided with a bell hidden function give lower prediction results than the networks with a tanh hidden function. For the networks with tanh hidden function, those provided with a linear output function give the best prediction results, with an optimum dimension of the hidden layer of four neurons.



**Table 4.** Leave-20%-Out Cross-Validation Results for the Estimation of the  $\alpha$ -sp<sup>2</sup>-CS with Neural Networks<sup>a</sup>

network specifications	<i>H</i>	<i>r</i> <sub>min</sub>	<i>r</i> <sub>max</sub>	<i>r</i> <sub>mean</sub>	<i>S</i> <sub>min</sub>	<i>S</i> <sub>max</sub>	<i>S</i> <sub>mean</sub>	<i>t</i> <sub>mean</sub> (s)
Act(Hidden)=tanh	1	0.9754	0.9799	0.9785	1.979	2.184	2.045	103
Act(Out)=linear	2	0.9843	0.9885	0.9870	1.502	1.751	1.594	408
	3	0.9868	0.9895	0.9884	1.434	1.604	1.504	1660
	4	0.9884	0.9916	0.9895	1.280	1.503	1.428	2828
	5	0.9873	0.9908	0.9888	1.345	1.577	1.476	4481
	6	0.9870	0.9914	0.9897	1.297	1.590	1.418	5987
Act(Hidden)=tanh	1	0.9729	0.9770	0.9752	2.116	2.292	2.193	345
Act(Out)=symlog	2	0.9832	0.9868	0.9847	1.603	1.809	1.727	551
	3	0.9843	0.9872	0.9863	1.580	1.748	1.633	1429
	4	0.9867	0.9893	0.9882	1.443	1.613	1.519	3395
	5	0.9860	0.9903	0.9884	1.379	1.652	1.506	4971
	6	0.9843	0.9899	0.9883	1.403	1.749	1.511	6831
Act(Hidden)=tanh	1	0.9730	0.9779	0.9756	2.073	2.287	2.174	254
Act(Out)=tanh	2	0.9838	0.9861	0.9850	1.649	1.779	1.712	536
	3	0.9828	0.9868	0.9859	1.606	1.833	1.655	1456
	4	0.9871	0.9889	0.9880	1.470	1.589	1.530	2534
	5	0.9865	0.9890	0.9880	1.465	1.624	1.528	4685
	6	0.9857	0.9905	0.9881	1.363	1.673	1.519	7112
Act(Hidden)=bell	1	0.9647	0.9790	0.9763	2.018	2.610	2.136	100
Act(Out)=linear	2	0.9801	0.9864	0.9836	1.627	1.970	1.782	613
	3	0.9759	0.9875	0.9818	1.560	2.162	1.873	1381
	4	0.9769	0.9870	0.9822	1.590	2.118	1.857	2034
	5	0.9756	0.9885	0.9846	1.498	2.178	1.721	3133
	6	0.9785	0.9918	0.9838	1.267	2.046	1.765	4276
Act(Hidden)=bell	1	0.9471	0.9787	0.9726	2.035	3.180	2.268	536
Act(Out)=symlog	2	0.9781	0.9875	0.9840	1.563	2.063	1.756	851
	3	0.9769	0.9859	0.9826	1.660	2.117	1.835	1662
	4	0.9736	0.9889	0.9819	1.472	2.261	1.866	2963
	5	0.9701	0.9896	0.9818	1.424	2.406	1.849	4066
	6	0.9801	0.9909	0.9857	1.337	1.968	1.662	6283
Act(Hidden)=bell	1	0.9494	0.9789	0.9696	2.025	3.113	2.390	749
Act(Out)=tanh	2	0.9791	0.9869	0.9839	1.598	2.018	1.766	887
	3	0.9733	0.9890	0.9828	1.466	2.276	1.816	1730
	4	0.9681	0.9864	0.9777	1.631	2.484	2.062	2883
	5	0.9562	0.9887	0.9794	1.483	2.902	1.954	4525
	6	0.9713	0.9870	0.9812	1.592	2.355	1.899	5577

<sup>a</sup> The notations are explained in Table 3.

Comparing the results reported in Tables 3 and 4 it is apparent that a (tanh, linear) network with four hidden neurons offers a good balance between calibration and prediction performances, while using more hidden neurons increases the computation time without improving the results. The calibration and prediction residuals for the four hidden neurons (tanh, linear) network are presented in Table 1, columns 12 and 13. From each set of ten simulations the best one was selected in calibration and prediction, respectively. As is apparent from Tables 3 and 4 the neural model gives good calibration and prediction results.

Investigated was the use of the mean of the predictions of the three networks with different pairs of activation functions and four hidden neurons in order to see if this combination of networks improves the predictions, as it was observed in a related investigation.<sup>28</sup> In the present case the statistical quality of the prediction did not change significantly with the use of the mean of the predictions.

**Outliers and Poorly Predicted Cases.** It is interesting to compare the number of  $\alpha$ -sp<sup>2</sup> carbons with a residual greater than a threshold for the networks with four hidden neurons and tanh hidden function. The threshold takes values between 1 and 4 ppm with a step of 0.5 ppm, and the calibration and cross-validation results are presented in Table 5. Also Table 5 reports the maximum negative and positive residual (MaxNegRes and MaxPosRes, respectively) together with the corresponding  $\alpha$ -sp<sup>2</sup> carbon. The prediction results indicate that the (tanh, linear) network has a lower number

of poorly predicted values than the other networks. In calibration carbon 150 has the MaxNegRes value, while the MaxPosRes value is exhibited by carbon 159 for (tanh, linear) and (tanh, symlog) networks and carbon 61 for the (tanh, tanh) network. For the cross-validation the MaxNegRes value is obtained for carbons 150, 167, and 168 for the networks with output function linear, symlog and tanh, respectively, while the MaxPosRes value is exhibited by carbon 159.

An inspection of the ANN residuals reported in Table 1 shows that the neural model gives excellent calibration and prediction results, with the exception of a small number of cases where the computed value differs significantly from the experimental chemical shift. In Table 6 there are presented the calibration and cross-validation outliers, carbons with a residual greater than three times the standard deviation. For calibration the (tanh, tanh) network has only two outliers, carbons 128 and 150, respectively. Carbon 150 is an outlier for all three networks, carbon 159 is an outlier for the (tanh, linear) and (tanh, symlog) networks, while carbon 128 is a common outlier for the (tanh, symlog) and (tanh, tanh) networks. For the cross-validation the (tanh, linear) network has the lowest number of outliers, namely carbons 89, 90, 150, and 159. Carbons 90 and 159 are common outliers for the three networks, carbon 150 is an outlier for the (tanh, linear) and (tanh, tanh) networks, while carbon 168 is a common outlier for the (tanh, symlog) and (tanh, tanh) networks. The outliers belong to highly

**Table 5.** Number of Poorly Predicted Cases at Different Levels of Accuracy by the Different Methods Investigated and the Minimum and Maximum Residual (MinRes and MaxRes, Respectively) in ppm<sup>a</sup>

method	accuracy level (ppm)							MaxNegRes	MaxPosRes
	1	1.5	2	2.5	3	3.5	4		
A. Calibration									
MLR	144	119	87	54	35	28	22	-16.7(158)	7.2(148)
tanh-linear	30	12	7	3	2	1	1	-3.5(150)	4.3(159)
tanh-symlog	43	21	12	4	1	1	0	-3.8(150)	2.5(159)
tanh-tanh	50	19	8	2	1	1	0	-3.9(150)	2.2(61)
B. Prediction by L20%O Cross-Validation for MLR and ANN and for the Chemical Shifts Computed with ChemWindows									
ChemWindows	137	111	71	44	33	29	21	-11.9(158)	8.4(242)
MLR	155	125	82	62	41	28	23	-17.6(158)	7.9(148)
tanh-linear	68	37	26	19	13	6	4	-4.0(150)	6.7(159)
tanh-symlog	75	52	26	21	16	12	7	-6.3(167)	5.9(159)
tanh-tanh	91	56	34	22	14	9	6	-5.3(168)	6.3(159)

<sup>a</sup> The index of the carbon atom with an extreme residual is indicated in parentheses. The neural networks are provided with four neurons in the hidden layer and different combinations of activation functions.

**Table 6.** Calibration and Cross-Validation Outliers and Their Residuals for the MLR Model and ANNs with Four Neurons in the Hidden Layer and Different Combinations of Activation Functions

method	no. of outliers	outliers (index, residual)
A. Calibration		
tanh-linear	4	(68,2.5),(125,-2.3),(150,-3.5),(159,4.3)
tanh-symlog	4	(128,-2.9),(130,-2.6),(150,-3.8),(159,2.5)
tanh-tanh	2	(128,-3.0),(150,-3.9)
MLR	3	(153,-11.5),(158,-16.7),(163,-11.5)
B. L20%O Cross-Validation		
tanh-linear	4	(89,4.0),(90,5.2),(150,-4.0),(159,6.7)
tanh-symlog	7	(68,5.0),(87,-6.0),(90,5.2),(149,-4.6),(159,5.9),(167,-6.3),(168,-4.4)
tanh-tanh	5	(90,5.7),(150,-4.5),(159,6.3),(165,4.6),(168,-5.3)
MLR	6	(131,-9.5),(153,-13.4),(158,-17.6),(163,-14.6),(165,-11.1),(237,-9.1)

branched alkenes: for atoms 150 and 159, C\* is a primary carbon atom with hydrogen atoms in the *cis* and *trans* positions and a highly branched *gem* carbon atom; atoms 89 and 90 belong to the same alkene with two *cis tert*-butyl and two *cis* methyl groups, atom 89 being quaternary and atom 90 primary; atom 168, from an alkene with four neopentyl groups.

After investigating the number of poorly predicted carbons and the number of outliers, it is clear that the (tanh, linear) network with four hidden neurons gives the best predictions for the  $\alpha$ -sp<sup>2</sup>-CS. This type of network was selected to further investigate the prediction of  $\alpha$ -sp<sup>2</sup>-CS.

**Comparison with MLR.** The main advantage of using neural networks in QSPR models is their capacity to offer a nonlinear mapping of the structural descriptors to the investigated physicochemical property. It is interesting to see how much is gained with ANNs in the prediction power of  $\alpha$ -sp<sup>2</sup>-CS in the present case. The neural model was compared with the MLR model obtained with the same set of structural descriptors. The MLR model was obtained using the same experimental data, topo-stereochemical descriptors, and cross-validation sets as those used in developing the neural models. The MLR calibration correlation coefficient *r* is equal to 0.961, and the standard deviation *s* is equal to 2.8 ppm, showing that the neural model is superior in calibration for the present case. The MLR L20%O cross-validation results (*r*<sub>cv</sub> = 0.952 and *s*<sub>cv</sub> = 3.0 ppm) show again that the neural models, even with one hidden neuron, provide better predictions than the linear model. Table 5 presents the number of poorly calculated  $\alpha$ -sp<sup>2</sup>-CS by the MLR model. From this table it is evident that both for calibration and prediction the MLR models has

a much larger number of poorly calculated  $\alpha$ -sp<sup>2</sup>-CS than the neural models presented in the same table. Comparing the number of calibration and cross-validation poorly calculated chemical shifts, it is clear that for the MLR model there is a small increase, demonstrating the stability in prediction for the MLR model. On the other hand, for the neural models there is a significant increase in the number of poorly calculated chemical shifts on passing from the calibration to the cross-validation, which indicates that the neural models is less stable in prediction, and extreme care must be exerted in order to obtain a good generalization and to avoid memorization of the patterns. The finding that the number of poorly predicted chemical shifts is much larger in the MLR model than in the neural model is a demonstration of the fact that there is a nonlinear relationship between the topo-stereochemical code of the  $\alpha$ -sp<sup>2</sup> carbon atom and its <sup>13</sup>C NMR chemical shift and that the neural networks used here are capable to capture such a relationship. For the MLR model there is a common pair of extreme carbons with an extreme residual both in calibration and in cross-validation, namely carbon 158 with a minimum residual and carbon 148 with a maximum residual. Table 6 presents the MLR statistical outliers: carbons 153, 158, and 163 in calibration and carbons 131, 153, 158, 163, 165, and 237 in cross-validation. The number of statistical outliers is not greater than in the case of neural model, but this is due to the greater standard deviation; the MLR residuals of the outliers are significantly greater than the ANN residuals, showing once again the superiority of the neural model in predicting  $\alpha$ -sp<sup>2</sup>-CS.

**Comparison with a General Additive Model.** The model developed in the present paper is directed to the

prediction of the <sup>13</sup>C NMR chemical shift of a single type of carbon atom, those situated in  $\alpha$  from a double bond. The results obtained in a previous paper show that such a kind of specific models can provide much better predictions than the general additive models in use for the prediction of the <sup>13</sup>C NMR chemical shift. Table 5 presents the number of poorly predicted values by the model developed by Pretsch<sup>38-41</sup> and implemented in the ChemWindows program.<sup>42</sup> The prediction results of this additive model are comparable with the results of the MLR model and much poorer than the results provided by the neural model. These results indicate that in the field of <sup>13</sup>C NMR chemical shift prediction general models are outperformed by more specific models, and in order to obtain better predictions it is worthy to pursue the effort to develop specific models for each kind of carbon environment. Also, the neural model has a proven superiority over the linear models, showing that there is a certain nonlinear dependence between the structural descriptors and the <sup>13</sup>C NMR chemical shift of  $\alpha$ -sp<sup>2</sup> carbons.

#### 4. CONCLUSION

In this paper was investigated a neural QSPR model for the estimation of the <sup>13</sup>C NMR chemical shift of sp<sup>3</sup> carbon atoms in the  $\alpha$  position relative to the double bond in acyclic alkenes. The structural description of the environment of the resonating carbon is made with a topo-stereochemical code which describes the number and relative position of carbon atoms around the resonating one. Four activation functions were tested in the neural model: the hyperbolic tangent or a bell-shaped function for the hidden layer and a linear, the symmetric logarithmoid, or a hyperbolic tangent function for the output layer. All combinations of activation functions give close results in the calibration of the ANN model, while for the prediction the (tanh, linear) network with four hidden neurons provides the best results. In a set of 10 simulations with different random initial weights the (tanh, linear) network with four hidden neurons gives consistent results, with a calibration standard deviation between 0.7 and 0.8 ppm and a cross-validation standard deviation between 1.3 and 1.5 ppm.

The results of the neural model were compared to those obtained with a multilinear regression model using the same set of structural descriptors. The MLR results in calibration ( $s = 2.8$  ppm) and cross-validation ( $s = 3.0$  ppm) show that the neural model provides a superior mapping of the topo-stereochemical code to the chemical shift of the investigated carbon atoms. By comparing the number of  $\alpha$ -sp<sup>2</sup> carbons with a residual greater than a threshold for the networks with four hidden neurons and the MLR model it was observed that the linear model has a larger number of poorly predicted chemical shifts, indicating that there is a nonlinear relationship between the topo-stereochemical code of the  $\alpha$ -sp<sup>2</sup> carbon atom and its <sup>13</sup>C NMR chemical shift and that the neural networks used here are capable to capture such a relationship in a simple and effective way.

The performances of the neural model were compared with the results offered by a general additive model for the estimation of the <sup>13</sup>C NMR chemical shift; the results of the additive model are comparable with the results of the MLR model and much poorer than the results provided by the neural model. The results obtained in this comparison together with earlier similar observations<sup>28</sup> indicate that for

the estimation of the <sup>13</sup>C NMR chemical shift general models are outperformed by more specific models, and in order to improve the predictions one possible avenue lies in the development of specific models for each type of carbon.

The topo-stereochemical code used provides a simple and comprehensive characterization of the environment of the resonating carbon. This finding is another argument for the use of a topo-stereochemical encoding of the atomic in the case of highly flexible molecules. The geometry of acyclic molecules presents many local minima, making it thus difficult to characterize in a simple way the local and global structure with geometric structural descriptors.

Recently proposed was a fuzzy model for the employment of the information contained in the <sup>13</sup>C NMR spectra.<sup>43,44</sup> This method can be used to estimate the carbon atom hybridization and  $\alpha$ -environment in the process of automated spectra interpretation or computer-assisted structure elucidation, giving a list of possible candidates. The approach developed in the present paper can be used to refine the list of candidates, by a feedback process of estimating the chemical shift of each candidate and comparing it with the starting value from the <sup>13</sup>C NMR spectra.

#### REFERENCES AND NOTES

- (1) Munk, M. E.; Madison, M. S.; Robb, E. W. The Neural Network as a Tool for Multispectral Interpretation. *J. Chem. Inf. Comput. Sci.* **1996**, *36*, 231-238.
- (2) Fessenden, R. J.; Györgyi, L. Identifying Functional Groups in IR Spectra Using an Artificial Neural Network. *J. Chem. Soc., Perkin Trans. 2* **1991**, 1755-1762.
- (3) Munk, M. E.; Madison, M. S.; Robb, E. W. Neural Network Models for Infrared Spectrum Interpretation. *Mikrochim. Acta* **1991**, *II*, 505-514.
- (4) Meyer, M.; Wiegelt, T. Interpretation of Infrared Spectra by Artificial Neural Networks. *Anal. Chim. Acta* **1992**, *265*, 183-190.
- (5) Weigel, U.-M.; Herges, R. Automatic Interpretation of Infrared Spectra: Recognition of Aromatic Substitution Patterns Using Neural Networks. *J. Chem. Inf. Comput. Sci.* **1992**, *32*, 723-731.
- (6) Tanabe, K.; Tamura, T.; Uesaka, H. Neural Network System for the Identification of Infrared Spectra. *Appl. Spectrosc.* **1992**, *46*, 807-810.
- (7) Ricard, D.; Cachet, C.; Cabrol-Bass, D.; Forrest, T. P. Neural Network Approach to Structural Feature Recognition from Infrared Spectra. *J. Chem. Inf. Comput. Sci.* **1993**, *33*, 202-210.
- (8) Meyer, M.; Meyer, K.; Hobert, H. Neural Networks for Interpretation of Infrared Spectra Using Extremely Reduced Spectral Data. *Anal. Chim. Acta* **1993**, *282*, 407-415.
- (9) Sbirrazzuoli, N.; Cachet, C.; Cabrol-Bass, D.; Forrest, T. P. Indices for the Evaluation of Neural Network Performance as Classifier: Application to Structural Elucidation in Infrared Spectroscopy. *Neural Comput. Applic.* **1993**, *1*, 229-239.
- (10) Cabrol-Bass, D.; Cachet, C.; Cleva, C.; Eghbaldar, A.; Forrest, T. P. Practical application of neural network research to spectral (infrared and mass) data for structural elucidation. *Can. J. Chem.* **1995**, *73*, 1412-1426.
- (11) Klawun, C.; Wilkins, C. L. Optimization of Functional Group Prediction from Infrared Spectra Using Neural Networks. *J. Chem. Inf. Comput. Sci.* **1996**, *36*, 69-81.
- (12) Curry, B.; Rumelhart, D. E. MSnet: A Neural Network which Classifies Mass Spectra. *Tetrahedron Comput. Methodol.* **1990**, *3*, 213-237.
- (13) Lohninger, H.; Stancl, F. Comparing the Performance of Neural Networks to Well-Established Methods of Multivariate Data Analysis: The Classification of Mass Spectral Data. *Fresenius J. Anal. Chem.* **1992**, *344*, 186-189.
- (14) Werther, W.; Lohninger, H.; Stancl, F.; Varmuza, K. Classification of Mass Spectra. A Comparison of Yes/No Classification Methods for the Recognition of Simple Structural Properties. *Chemom. Intell. Lab. Syst.* **1994**, *22*, 63-76.
- (15) Eghbaldar, A.; Forrest, T. P.; Cabrol-Bass, D.; Cambon, A.; Guignonis, J.-M. Identification of Structural Features from Mass Spectrometry Using a Neural Network Approach: Application to Trimethylsilyl Derivatives Used for Medical Diagnosis. *J. Chem. Inf. Comput. Sci.* **1996**, *36*, 637-643.

- (16) Klawun, C.; Wilkins, C. L. Joint Neural Network Interpretation of Infrared and Mass Spectra. *J. Chem. Inf. Comput. Sci.* **1996**, *36*, 249–257.
- (17) Jurs, P. C.; Ball, J. W.; Anker, L. S.; Friedman, T. L. Carbon-13 Nuclear Magnetic Resonance Spectrum Simulation. *J. Chem. Inf. Comput. Sci.* **1992**, *32*, 272–278.
- (18) Kvasnicka, V. An Application of Neural Networks in Chemistry. Prediction of  $^{13}\text{C}$  NMR Chemical Shifts. *J. Math. Chem.* **1991**, *6*, 63–76.
- (19) Doucet, J. P.; Panaye, A.; Feuillebois, E.; Ladd, P. Neural Networks and  $^{13}\text{C}$  NMR Shift Prediction. *J. Chem. Inf. Comput. Sci.* **1993**, *33*, 320–324.
- (20) Panaye, A.; Doucet, J. P.; Fan, B. T.; Feuillebois, E.; El Azzouzi, S. R. Artificial Neural Network Simulation of  $^{13}\text{C}$  NMR Shifts for Methyl Substituted Cyclohexanes. *Chemom. Intell. Lab. Syst.* **1994**, *24*, 129–135.
- (21) Ivanciuc, O. Artificial Neural Networks Applications. Part 6. Use of Non-Bonded van der Waals and Electrostatic Intramolecular Energies in the Estimation of  $^{13}\text{C}$  NMR Chemical Shifts in Saturated Hydrocarbons. *Rev. Roum. Chim.* **1995**, *40*, 1093–1101.
- (22) Kvasnicka, V.; Sklenák, Š.; Pospíchal, J. Application of Recurrent Neural Networks in Chemistry. Prediction and Classification of  $^{13}\text{C}$  NMR Chemical Shifts in a Series of Monosubstituted Benzenes. *J. Chem. Inf. Comput. Sci.* **1992**, *32*, 742–747.
- (23) Kvasnicka, V.; Sklenák, Š.; Pospíchal, J. Application of Neural Networks with Feedback Connections in Chemistry: Prediction of  $^{13}\text{C}$  NMR Chemical Shifts in a Series of Monosubstituted Benzenes. *J. Mol. Struct. (Theochem)* **1992**, *277*, 87–107.
- (24) Anker, L. S.; Jurs, P. C. Prediction of Carbon-13 Nuclear Magnetic Resonance Chemical Shifts by Artificial Neural Networks. *Anal. Chem.* **1992**, *64*, 1157–1164.
- (25) Miyashita, Y.; Yoshida, H.; Yaegashi, O.; Kimura, T.; Nishiyama, H.; Sasaki, S. Non-Linear Modelling of  $^{13}\text{C}$  NMR Chemical Shift Data Using Artificial Neural Networks and Partial Least Squares Method. *J. Mol. Struct. (Theochem)* **1994**, *311*, 241–245.
- (26) Mitchell, B. E.; Jurs, P. C. Computer Assisted Simulations of  $^{13}\text{C}$  Nuclear Magnetic Spectra of Monosaccharides. *J. Chem. Inf. Comput. Sci.* **1996**, *36*, 58–64.
- (27) Clouser, D. L.; Jurs, P. C. Simulation of the  $^{13}\text{C}$  Nuclear Magnetic Resonance Spectra of Ribonucleosides Using Multiple Linear Regression Analysis and Neural Networks. *J. Chem. Inf. Comput. Sci.* **1996**, *36*, 168–172.
- (28) Ivanciuc, O.; Rabine, J.-P.; Cabrol-Bass, D.; Panaye, A.; Doucet, J. P.  $^{13}\text{C}$  NMR Chemical Shift Prediction of  $\text{sp}^2$  Carbon Atoms in Acyclic Alkenes Using Neural Networks. *J. Chem. Inf. Comput. Sci.* **1996**, *36*, 644–653.
- (29) Panaye, A.; Doucet, J. P.; Fan, B. T. Topological Approach of  $\text{C}13$  NMR Spectral Simulation: Application to Fuzzy Substructures. *J. Chem. Inf. Comput. Sci.* **1993**, *33*, 258–265.
- (30) Kreinovich, V. Arbitrary Nonlinearity is Sufficient to Represent all Functions by Neural Networks: A Theorem. *Neural Networks* **1991**, *4*, 381–384.
- (31) Bulsari, A. B.; Saxén, H. System Identification of a Biochemical Process Using Feed-Forward Neural Networks. *Neurocomputing* **1991**, *3*, 125–133.
- (32) Bulsari, A. B.; Saxén, H. System Identification Using the Symmetric Logarithmoid as an Activation Function in a Feed-Forward Neural Network. *Neural Network World* **1991**, *4*, 221–224.
- (33) Rumelhart, D. E.; Hinton, G. E.; Williams, R. J. Learning Representations by Back-Propagating Errors. *Nature* **1986**, *323*, 533–536.
- (34) Cybenko, G. Approximations by Superpositions of a Sigmoidal Function. *Math. Control Signals Syst.* **1989**, *2*, 303–314.
- (35) Funahashi, K. On the Approximate Realization of Continuous Mappings by Neural Networks. *Neural Networks* **1989**, *2*, 183–192.
- (36) Hornik, K.; Stinchcombe, M.; White, H. Multilayer Feedforward Networks are Universal Approximators. *Neural Networks* **1989**, *2*, 359–366.
- (37) Hornik, K.; Stinchcombe, M.; White, H. Universal Approximation of an Unknown Mapping and Its Derivatives Using Multilayer Feedforward Networks. *Neural Networks* **1990**, *3*, 551–560.
- (38) Fürst, A.; Pretsch, E. A Computer Program for the Prediction of  $^{13}\text{C}$ -NMR Chemical Shifts of Organic Compounds. *Anal. Chim. Acta* **1990**, *229*, 17–25.
- (39) Fürst, A.; Pretsch, E.; Robien, W. Comprehensive Parameter Set for the Prediction of the  $^{13}\text{C}$ -NMR Chemical Shifts of  $\text{sp}^3$ -Hybridized Carbon Atoms in Organic Compounds. *Anal. Chim. Acta* **1990**, *233*, 213–222.
- (40) Pretsch, E.; Fürst, A.; Robien, W. Parameter Set for the Prediction of the  $^{13}\text{C}$  NMR Chemical Shifts of  $\text{sp}^2$ - and  $\text{sp}$ -Hybridized carbon Atoms in Organic Compounds. *Anal. Chim. Acta* **1991**, *248*, 415–428.
- (41) Pretsch, E.; Fürst, A.; Badertscher, M.; Bürgin, R.; Munk, M. E. C13Shift: A Computer Program for the Prediction of  $^{13}\text{C}$  NMR Spectra Based on an Open Set of Additivity Rules. *J. Chem. Inf. Comput. Sci.* **1992**, *32*, 291–295.
- (42) ChemWindows; SoftShell International, Inc.: 715 Horizon Dr., Ste. 390, Grand Junction, CO 81506-8727.
- (43) Laidboeur, T.; Laude, I.; Cabrol-Bass, D.; Bangov, I. P. Employment of Fuzzy Information Derived from Spectroscopic Data toward Reducing the Redundancy in the Process of Structure Generation. *J. Chem. Inf. Comput. Sci.* **1994**, *34*, 171–178.
- (44) Bangov, I. P.; Laude, I.; Cabrol-Bass, D. Combinatorial Problems in the Treatment of Fuzzy  $^{13}\text{C}$  NMR Spectral Information in the Process of Computer-Aided Structure Elucidation: Estimation of the Carbon Atom Hybridization and  $\alpha$ -Environment States. *Anal. Chim. Acta* **1994**, *298*, 33–52.

CI9601574